Title: PREDICTION OF PRIMARY SOMATOSENSORY NEURON ACTIVITY DURING ACTIVE TACTILE EXPLORATION

Authors: Dario Campagner[1], Mathew Evans[1], Michael R. Bale[1,2], Andrew Erskine[1,3], Rasmus S. Petersen[1]

Authors' affiliation: 1. Faculty of Life Sciences, University of Manchester, Stopford Building, Oxford Road, Manchester M13 9PT, UK. 2. School of Life Sciences, University of Sussex, Brighton, BN1 9QG, UK 3. National Institute for Medical Research (NIMR), The Ridgeway, Mill Hill, London, UK.

Correspondence to: R.Petersen@manchester.ac.uk

ABSTRACT

Primary sensory neurons form the interface between world and brain. Their function is well-understood during passive stimulation but, under natural behaving conditions, sense organs are under active, motor control. In an attempt to predict primary neuron firing under natural conditions of sensorimotor integration, we recorded from primary mechanosensory neurons of awake, head-fixed mice as they explored a pole with their whiskers, and simultaneously measured both whisker motion and forces with high-speed videography. Using Generalised Linear Models, we found that primary neuron responses were poorly predicted by kinematics but well-predicted by rotational forces acting on the whisker: both during touch and free-air whisker motion. These results are discrepant with previous studies of passive stimulation, but could be reconciled by differences in the kinematics-force relationship between active and passive conditions. Thus, simple statistical models can predict rich neural activity elicited by natural, exploratory behaviour involving active movement of the sense organs.

INTRODUCTION

A major challenge of sensory neuroscience is to understand the encoding properties of neurons to the point that their spiking activity can be predicted in the awake animal, during natural behaviour. However, accurate prediction is difficult without experimental control of stimulus parameters and, despite early studies of awake, behaving animals (Hubel, 1959), subsequent work has most often effected experimental control by employing anaesthesia and/or passive stimulation. However, the active character of sensation (Gibson, 1962; Yarbus 1967), based on motor control of the sense organs, is lost in reduced preparations. Recent methodological advances permit a way forward: in the whisker system, it is now possible to record neuronal activity from an awake mouse, actively exploring the environment with its whiskers, whilst simultaneously measuring the fundamental sensory variables (whisker kinematics and mechanics) likely to influence neuronal activity (O'Connor et al 2010).

Our aim here was to predict spikes fired by primary whisker neurons (PWNs) of awake mice engaged in natural, object exploration behaviour. The manner in which primary neurons encode sensory information fundamentally constrains all downstream neural processing (Lettvin et al. 1959). PWNs innervate mechanoreceptors located in the whisker follicles (Zucker and Welker 1969; Rice et al. 1986) and project to the cerebral cortex, analogously to other modalities, via trisynaptic pathways through the brainstem and thalamus (Diamond et al. 2008). Here, we show that primary neuron responses are well-predicted by a rotational force ('moment') acting on the whisker, but not by whisker angle and its derivatives – a finding at odds with passive stimulation studies (Gibson 1983, Lichtenstein et al 1990; Bale et al 2013).

RESULTS:

Primary whisker neuron activity during object exploration is predicted by whisker bending moment

We recorded the activity of single PWNs from awake mice (Figure 1A, E`, Figure 1-figure supplement 1) as they actively explored a metal pole with their whiskers (N = 20 units). At the same time, we recorded whisker motion and whisker shape using high-speed videography (1000 frames/s, Figure 1D, Figure 1-figure supplement 2). Since each PWN innervates a single whisker follicle, we tracked the 'principal whisker' of each recorded unit from frame to frame, and extracted both the angle and curvature of the principal whisker in each video frame (total 1,496,033 frames; Figure 1B-E; Bale et al. 2015). Whiskers are intrinsically curved, and the bending moment on a whisker is proportional to how much this curvature changes due to object contact (Birdwell et al. 2007): we therefore used 'curvature change' as a proxy for bending moment (O'Connor et al. 2010a). Whisker-pole contacts caused substantial whisker bending (curvature change), partially correlated with the whisker angle (Figures 1E, 4E) and, consistent with Szwed et al. (2003) and Leiser and Moxon (2007), robust spiking (Figures 1E, 2E).

To test between candidate encoding variables, our strategy was to determine how accurately it was possible to predict PWN activity from either the angular position (kinematics) or curvature change (mechanics) of each recorded unit's principal whisker. To predict spikes from whisker state, we used Generalised Linear Models (GLMs) (Figure 2A). GLMs, driven by whisker angle, have previously been shown to provide a simple but accurate description of the response of PWNs to passive stimulation (Bale et al. 2013) and have mathematical properties ideal for robust parameter-fitting (Truccolo et al. 2005; Paninski et al. 2007).

For each recorded unit (median 69,672 frames and 550 spikes per unit), we computed the GLM parameters that maximised the regularised likelihood of the unit's spike train given the whisker angle time series (8 fitted parameters) and assessed the quality of the best-fitting GLM by feeding it with the whisker angle time series as input and generating a predicted spike train in response (using cross-validation). We then compared the recorded spike train to the GLM-predicted one (Figure 2B-C) and quantified the similarity between the smoothed spike trains using the Pearson correlation coefficient (PCC). This is a stringent, single-trial measure of model prediction performance (Figure 2-figure supplement 1B). We then repeated this entire procedure for the whisker curvature time series. Although angle GLMs predicted spike trains of a few units moderately well (2/20 units had PCC > 0.5), they performed poorly for the majority (median PCC 0.06, IQR 0.019-0.3; Figure 2B-D, orange). This was not simply because of non-linear tuning to whisker angle, since quadratic GLMs fared only marginally better (median PCC 0.097, IQR 0.042-0.31; p=0.044, signed-rank test, Figure 2-figure supplement 1A). In contrast, we found that the curvature GLMs were substantially more accurate than the angle GLMs (median PCC 0.52, IQR 0.22-0.66; p=0.0044, signed-rank test; Figure 2B-D, blue) with prediction accuracy up to PCC 0.88. This result was robust to the number of fitted parameters: a GLM sensitive to instantaneous curvature exhibited very similar prediction accuracy (Figure 2-figure supplement 1C).

Although the activity of most units was better predicted by whisker curvature change than by whisker angle, there were a few units for which the angle prediction performance was appreciable (Figure 2D). However, we found that this could largely be attributed to redundancy. When a mouse whisks against an object, curvature change and angle fluctuate in concert (Birdwell et al. 2007; Bagdasarian et al. 2013; Pammer et al. 2013; Figures 1E, 4E and Figure 4-figure supplement 1). When we fitted GLMs using both curvature change and angle as input, these GLMs predicted the spike trains no more accurately (median PCCs 0.53

IQR 0.40-0.62; p=0.067, signed-rank test; Figure 2D) than GLMs based on curvature change alone.

In principle, neurons might also be sensitive to the axial force component (parallel to the whisker follicle) and/or lateral force component (orthogonal to axial) associated with whisker-object contact (Figure 1B-C; Solomon and Hartmann, 2011; Pammer et al. 2013). We restricted our analysis to bending moment since, under our experimental conditions, axial/lateral force components were near-perfectly correlated with bending moment (Figure 2-figure supplement 2) and bending moment is likely to have a major influence on stresses in the follicle due to mechanical advantage (Pammer et al. 2013).

To further test the curvature-encoding concept, we asked whether curvature GLMs could account for the response of PWNs to whisker-pole touch. To this end, we parsed the video data into episodes of 'touch' and 'non-touch'. Units fired at a higher rate during touch than otherwise (Szwed et al. 2003; Leiser and Moxon, 2007). Without any further parameter-adjustment, the curvature-based GLMs reproduced this effect (Figure 2E): the correlation coefficient between recorded and GLM-predicted firing rate for touch episodes was 0.96. Collectively, the above results indicate that, during active touch, the best predictor of whisker primary afferent firing is not a kinematic parameter (whisker angle or its derivatives), as has been consistently reported in studies using passive stimulation, but rather a mechanical parameter – the bending moment.

Primary whisker neuronal activity during whisking is predicted by moment

During free whisking - in the absence of whisker-pole contact - whisker curvature, and therefore bending moment, changed little (Figure 1E, Figure 4-supplement figure 1A); consistent with previous studies (Knutsen et al. 2008; Quist et al. 2014). Yet, 50% of recorded units ('whisking-sensitive units') were significantly modulated by whisking

amplitude (Figure 3A). This suggests that moment due to whisker bending is not the only force that influences afferent activity. A likely candidate is the moment associated with the rotational motion of a whisker: this 'inertial' moment is proportional to the whisker's angular acceleration (Quist et al. 2014). Consistent with this possibility, we found that whisking-sensitive units were tuned to angular acceleration (Figure 3B) and that 60% of these were phase-modulated (Figure 3C). Angular acceleration tuning was diverse: some units fired to acceleration in a particular direction (rostral or caudal), whilst others responded to acceleration in both directions (Figure 3B). Moreover, for whisking-sensitive units (but not the whisking-insensitive ones), quadratic GLMs trained on data from non-touch episodes were able to predict spikes using whisker angle acceleration as input (Figure 3D-E; whisking sensitive units, median PCC 0.38, IQR 0.22-0.56; non-whisking sensitive median PCC -0.006, IQR -0.03-0.03, p=0.001 rank-sum test). These findings indicate that, in the absence of whisker-object contact, responses of PWNs to whisking itself can be accounted for by sensitivity to the moment associated with angular whisker acceleration.

Relation between kinematics and mechanics is different in active vs passive touch and has implications for neural encoding

We found, during active object exploration, that bending moment, but not whisker angle, predicts PWN firing. In apparent contrast, studies using the acute, passive stimulation paradigm have reported that PWNs encode whisker angle (and its temporal derivatives, Zucker and Welker, 1969; Gibson and Welker, 1983; Lichtenstein et al. 1990; Jones et al. 2004; Arabzadeh et al. 2005; Bale and Petersen, 2009; Lottem and Azouz, 2011; Bale et al., 2013). We wondered whether the discrepancy might be due to differences in whisker mechanics between passive and active stimulation conditions. To test this, we analysed the

relationship between angle and curvature change during active touch and compared it to that during passive whisker stimulation. During active pole exploration, angle and curvature change were, over all, only loosely related (median correlation coefficient 0.20, IQR 0.079-0.39, Figures 4D-E). Important contributory factors were that the angle-curvature relationship was both different for touch compared to non-touch (Figure 4-figure supplement 1A) and dependent on object location (Figure 4- figure supplement 1B). In contrast, during passive stimulation, whisker angle was near perfectly correlated with curvature change (for C2, correlation coefficients 0.96 and 0.94 respectively; similar results for C5; Figures 4C-D and Figure 4E, inset); consistent with properties of cantilevered beams (Birdwell et al., 2007). Simulations confirmed that, due to the tight relationship between the variables, a unit tuned only to curvature change can appear tightly tuned to angle (Figure 4- figure supplement 2). The implication is that apparent sensitivity to whisker angle under passive stimulation conditions can be accounted for by moment-tuning.

DISCUSSION

Prediction of spikes fired by sensory neurons under natural conditions

In the endeavour to understand how neurons encode and process sensory information, there is a basic tension between the desire for tight experimental control and the desire to study animals under natural, unconstrained conditions. Theories of sensory encoding suggest that neural circuits have evolved to operate efficiently under natural conditions (Simoncelli and Olshausen, 2001; Reinagel 2001). Previous studies have succeeded in predicting/decoding spikes evoked by passive presentation of natural sensory stimuli to anaesthetised/immobilised animals (Lewen et al. 2001; Arabzadeh et al. 2005; Pillow et al. 2008; Mante et al. 2008; Lottem and Azouz, 2011; Bale et al., 2013), but it has been difficult to extend this approach

to encompass natural, active movement of the sense organs. Here we have addressed this general issue, taking advantage of experimental possibilities recently created in the whisker system (O'Connor et al, 2010a), and the ability of computational methods to uncover stimulus-response relationships even from data with complex statistical structure (Paninski et al., 2007; Fairhall and Sompolinski, 2014). Our main finding was that responses of PWNs, recorded as an awake mouse actively explores an object with its whiskers, can be predicted from the forces acting on the whiskers. Given that, for each unit, we were attempting to predict the entire ~70 s time course of activity, the variability of the behaviour of untrained mice (O'Connor et al., 2010a), and the lack of trial-averaging as a noise reduction strategy, it is remarkable that we found model prediction correlation coefficients up to 0.88.

Mechanical framework for tactile coding

Our finding of force-encoding is at odds with previous passive stimulation studies but consistent with previous studies using electrical whisking and biomechanical modelling. Pushing a whisker against an object triggers spiking in many PWNs (Szwed et al. 2003, 2006; Leiser and Moxon, 2007). Modelling by Hartmann and co-workers accounts for this by a biomechanical framework where the whisker is conceptualised as an elastic beam, cantilever-mounted in the skin (Birdwell et al. 2007; Quist et al. 2014). When such a beam pushes against an object, the beam bends, causing reaction forces at its base. Our data are in striking agreement with the general suggestion that mechanoreceptor activity is closely related to such reaction forces. Previous studies reported that PWNs encode both whisker-object contact and whisker motion itself (Szwed et al. 2003; Leiser and Moxon, 2007; Khatri et al. 2009). Our results show that moment associated both with contact-induced whisker bending and with whisker rotation predicts PWN spiking. Thus, a common framework accounts for diverse PWN properties.

In apparent contrast, previous studies using passive stimulation in anaesthetised animals have consistently reported a tight relationship between whisker kinematics and PWN response. In the cantilever whisker model, passively induced changes in whisker angle correlate highly with whisker bending. We confirmed that this applies to real whiskers *in vivo* and demonstrate that moment-sensitive units can thereby appear angle-tuned. In this way, moment-encoding can account for primary neuron responses not only during active touch but also under passive stimulation. More generally, our results highlight the importance of studying neurons under natural, active sensing conditions.

It is axiomatic that mechanoreceptors are sensors of internal forces acting in the tissue within which they are embedded (Abraira and Ginty, 2013) and therefore valuable to be able to measure mechanical forces in the awake, behaving animal. In general, including the important case of primate hand-use, the complex biomechanics of skin makes force-estimation difficult (Phillips and Johnson, 1981). In contrast, for whiskers, the quasi-static relationship is relatively simple: the bending moment on a whisker is proportional to its curvature and this has the important implication that reaction forces can be directly estimated from videography *in vivo* (Birdwell et al. 2007; O'Connor et al. 2010a; Pammer et al. 2013). Our results are the first direct demonstration that such reaction forces drive primary sensory neuron responses – likely involving Piezo2 ion channels (Woo et al. 2014; Poole et al. 2015; Whiteley et al. 2015). Our findings show that sensitivity to touch and self-motion in the somatosensory pathway (Curtis and Kleinfeld, 2009; O'Connor et al. 2010b; Curtis and Kleinfeld, 2009; Huber et al. 2012; Petreanu et al. 2012; Peron et al. 2015), arises directly at receptor level, indicating a direct connection from receptor mechanisms to behaviour.

Moment-based computations in tactile behaviour

Extraction of bending moment is a useful first step for many tactile computations. Large transients in bending moment signal object-touch events, and the magnitude of bending is inversely proportional to the radial distance of contact along the whisker (Solomon and Hartmann, 2006). As illustrated by our results on the statistics of active touch, if integrated with cues for whisker self-motion, whisker bending can be a cue to the 3D location of an object (Szwed et al. 2003, Szwed et al. 2006, Birdwell et al. 2007; Bagdasarian et al 2013; Pammer et al., 2013). Bending moment can permit wall following (Sofroniew et al., 2014) and, if integrated across whiskers, can in principle be used both to infer object shape (Solomon and Hartmann, 2006) and to map the spatial structure of the environment (Fox et al., 2012, Pearson et al., 2013).

Summary and Conclusion

We have shown that the responses of primary whisker neurons can be predicted, during natural behaviour that includes active motor control of the sense organ, from forces acting on the whiskers. These results provide a bridge linking receptor mechanisms to behaviour.

EXPERIMENTAL PROCEDURES

All experimental protocols were approved by both United Kingdom Home Office national authorities and institutional ethical review.

Surgical procedure

Mice (C57; N=10; 6 weeks at time of implant) were anesthetized with isoflurane (2% by volume in O_2), mounted in a stereotaxic apparatus (Narishige) and body temperature maintained at 37°C using a homeothermic heating system. The skull was exposed and a titanium head-bar (19.1mm x 3.2mm x 1.3mm; O'Connor et al., 2010a) was first attached to the skull ~1 mm posterior to lambda (Vetbond), and then fixed in place with dental acrylic (Lang dental). A craniotomy was made (+0.5mm to -1.5mm posterior to bregma, 0mm to 3mm lateral) and sealed with silicone elastomer. Buprenorphine (0.1 mg/kg) was injected subcutaneously for postoperative analgesia and the mouse left to recover for at least 5 days

Behavioural apparatus

The behavioural apparatus was adapted from O'Connor et al. (2010a). A mouse was placed inside a perspex tube (inner diameter 32 mm), from which its head emerged at one end, and immobilised by fixing the head-bar to a custom mount holder. The whiskers were free of the tube at all times. The stimulus object was a 1.59 mm diameter metal pole, located ~3.5mm lateral to the mouse's snout. To allow control of its anterior/posterior location, the pole was mounted on a frictionless linear slide (Schneeberger NDN 2-50.40) and coupled to a linear stepper motor (Zaber NA08B30). To allow vertical movement of the pole into and out of range of the whiskers, the pole/ actuator assembly was mounted on a pneumatic linear slide (Festo SLS-10-30-P-A), powered by compressed air. The airflow was controlled by a relay

(Weidmüller). In this way, the pole moved rapidly (~0.15 s) into and out of range of the whiskers. The apparatus was controlled from Matlab via a real-time processor (TDT, RX8).

Electrophysiology

To permit reliable whisker tracking (see below), before each recording session, A, B and E whisker rows were trimmed to the level of the fur, under brief isoflurane anaesthesia. The trigeminal ganglion was targeted as previously described (Bale et al., 2015). The silicone seal was removed and a 3/4 shank tungsten microelectrode array (FHC, recording electrodes 8MΩ at 1kHz, reference 1MΩ; tip spacing ~500 μm) was lowered through the brain (angle 4 ° to vertical in the coronal plane) using a micromanipulator (Scientifica, PatchStar) under isoflurane anaesthesia. Extracellular potentials were pre-amplified, digitised (24.4 kHz), filtered (band pass 300-3000 Hz) and acquired continuously to hard disk (TDT, RZ5). The trigeminal ganglion was encountered 6-7 mm vertically below the pial surface and whisker-response units identified by manual deflection of the whiskers with a small probe. Once a well-isolated unit was found, the whisker that it innervated (the 'principal whisker') was identified by manual stimulation. At this point, anaesthesia was discontinued. Once the mouse was awake, we recorded neuronal activity during repeated presentations of the pole ('trials'). Before the start of each trial, the pole was in the down position, out of reach of the whiskers. The pole was first moved anterior-posteriorly to a position chosen randomly out of a set of 11 possible positions, spanning a range ±6 mm with respect to the resting position of the base of the principal whisker. A trial was initiated by activating the pneumatic slide relay, thus moving the pole up into the whisker field, where it remained for 3s before being lowered. At the end of a recording session, the microelectrode array was withdrawn, the craniotomy sealed with silicone elastomer, and the mouse returned to its home cage.

High-speed videography

Using the method of O'Connor et al. (2010a) to image whisker movement/shape, whiskers ipsilateral to the recorded ganglion were illuminated from below using a high-power infrared LED array (940 nm; Roithner, LED 940-66-60) via a diffuser and condensing lens. The whiskers were imaged through a telecentric lens (Edmunds Optics, 55-349) mounted on a high speed camera (Mikrotron, LTR2; 1000 frames/s, 0.4 ms exposure time). The field of view of the whiskers was 350x350 pixels, with pixel width 0.057mm.

Response to touch and non-touch events

Mouse whisking behaviour during the awake recording was segmented into 'touch', and 'non-touch' episodes. Touches between the principal whisker of each unit and the pole were scored manually in each frame of the high-speed video. Any frame not scored as a touch was scored as non-touch. Touch and non-touch firing rates for a given unit were computed by averaging activity over all corresponding episodes.

Whisker tracking

Since the trigeminal ganglion lacks topography, it is difficult to target units that innervate a specific whisker, and therefore desirable for a whisker tracker to be robust to the presence of multiple rows of whiskers. However, since neurons in the ganglion innervate individual whiskers, it is sufficient to track only one whisker (the principal one) for each recorded neuron. To extract kinematic/mechanical whisker information, we therefore developed a whisker tracker ('WhiskerMan'; Bale et al., 2015) whose design criteria, different to those of other trackers (Perkon et al., 2011; Clack et al., 2012), were to: (1) be robust to whisker cross-over events; (2) track a single, target whisker; (3) track the proximal segment of the whisker shaft. The shape of the target whisker segment was described by a quadratic Bezier curve $\mathbf{r}(t,s)$ (a good approximation away from the zone of whisker-object contact; Quist et al., 2012; Pammer et al., 2013): $\mathbf{r}(t,s) = [x(t,s), y(t,s)]$, where x, y are horizontal/vertical

coordinates of the image, s = [0,..,1] parameterises (x,y) location along the curve and t is time. We fitted such a Bezier curve to the target whisker in each image frame using a local, gradient-based search. The initial conditions for the search were determined by extrapolating the solution curves from the previous two frames, assuming locally constant, angular velocity. The combination of the low-parameter whisker description and the targeted, local search makes the algorithm robust to whisker cross-over events. The 'base' of the target whisker was defined as the intersection between the extrapolated Bezier curve and the snout contour (estimated as described in Bale et al., 2015). The solution curve in each frame was visually checked and the curves manually adjusted to correct occasional errors.

Estimation of kinematic/force parameters

The whisker angle (θ) in each frame was measured as the angle between the tangent to the whisker curve at the base and the anterior-posterior axis (Figure 1B). Whisker curvature (κ) was measured at the base as $\kappa = \frac{x'y''-x''y'}{(x'^2+y'^2)^{3/2}}$, where x', y' and x'', y'' are the first and second partial derivatives of the functions $x(s)$ and $y(s)$ with respect to s (Figure 1B). Since reaction force at the whisker base reflects changes in whisker curvature, rather than the intrinsic (unforced) curvature (Birdwell et al., 2007), we computed 'curvature change' $\Delta\kappa = \kappa - \kappa_{int}$, where κ_{int}, the intrinsic curvature, was estimated as the average of κ in the first 100 ms of the trial (before pole contact; O'Connor et al., 2010a). During free whisking, whisker angle oscillated with the characteristic whisking rhythm, but curvature changed little. The small changes in whisker curvature during free whisking were consistent with torsional effects (Knutsen et al. 2008).

Under conditions of whisking against a smooth surface, such as in the present study, the frictionless quasi-static framework of Birdwell et al. (2007) applies, and bending moment is proportional to Δκ. We estimated bending moment using the method of Pammer et al. (2013)

from $\Delta\kappa$, using the radius of the relevant whisker at the base and published data on Young's modulus of mouse whiskers (Quist and Hartmann, 2012).

Axial ($\vec{F}_{ax}$) and lateral forces ($\vec{F}_{lat}$) at the whisker base were calculated, during periods of whisker-pole contact, using the method of Pammer et al. (2013), from bending moment and whisker-pole contact location. Pole location, in the horizontal plane, in each frame, was identified as the peak of a 2D convolution between the video image and a circular pole template. To localise whisker-pole contact, the whisker tracker was used to fit the distal segment of the whisker close to the pole, seeded by extrapolation from the whisker tracking solution for the proximal whisker segment, described above. Whisker-pole contact location was defined as the point where this distal curve segment was closest to the detected pole centre. Pole and contact locations were verified by visual inspection.

The 'inertial' moment associated with the rotational motion of a whisker is proportional to angular acceleration (Quist et al. 2014). To quantify inertial moment during free whisking, we therefore used angular whisker acceleration as a proxy. Acceleration was calculated from the whisker angle time series after smoothing with a Savitzky-Golay filter (polynomial order 5; frame size 31 ms).

Passive whisker deflection

To determine how whiskers move/bend in response to passive deflection under anaesthesia, a mouse was anesthetized (isoflurane 2%) and placed in the head-fixation apparatus. Individual whiskers (C2 and C5, trimmed to 5 mm) were mechanically deflected using a piezoelectric actuator as previously described (Bale et al., 2013; Bale et al. 2015). All other whiskers were trimmed to the level of the fur. Each whisker, in turn, was inserted into a snugly fitting plastic

tube attached to the actuator, such that the whisker entered the tube 2 mm from the face. Two stimuli were generated via a real-time processor (TDT, RX8): (1) a 10 Hz trapezoidal wave (duration 3 s, amplitude 8 °); (2) Gaussian white noise (duration 3 s, smoothed by convolution with a decaying exponential: time constant 10 ms; amplitude SD 2.1 °). During the stimulation, the whiskers were imaged as detailed above (1000 frames/s, 0.2 ms exposure time).

Electrophysiological data analysis

Spike sorting: Single units were isolated from the extracellular recordings as previously described, by thresholding and clustering in the space of 3-5 principal components using a mixture model (Bale and Petersen, 2009). A putative unit was only accepted if (1) its inter-spike interval histogram exhibited a clear absolute refractory period and (2) its waveform shape was consistent between the anaesthetised and awake phases of the recording.

Responses to whisking without touch: To test whether a unit responded to whisking itself, we extracted non-touch episodes as detailed above and computed time series of whisking amplitude and phase by band-pass filtering the whisker angle time series (6-30Hz) and computing the Hilbert transform (Kleinfeld and Deschênes 2011). Amplitudes were discretised (30 equi-populated bins) and the spiking data used to compute amplitude tuning functions. Phases for bins where the amplitude exceeded a given threshold were discretised (8 equi-populated bins) and used to construct phase tuning functions. To determine whether a unit was significantly amplitude-tuned, we fitted a regression line to its amplitude tuning curve and tested whether the slope was statistically significantly different to 0 ($p=0.0025$, Bonferroni corrected). To determine whether a unit was significantly phase-tuned, we computed the maximum value of its phase tuning curve and compared this to the distribution of maxima of chance tuning functions. Chance tuning functions were obtained by randomly shifting the recorded spike sequences by 3000-8000 ms and recomputing tuning functions

(500 times). A unit was considered phase-tuned if its tuning function maximum (computed using amplitude threshold of 2°) exceeded the 95th percentile of the shuffled distribution.

Generalised Linear Model (GLM): To investigate how well primary whisker neurons encode a given sensory variable (e.g., whisker angle, curvature), we fitted single unit activity to a GLM (Nelder and Wedderburn, 1972; Truccolo et al., 2005; Paninski et al., 2007), similarly to Bale et al. (2013). For each unit, a 'stimulus' time series (x) (whisker angle or whisker curvature change) and a simultaneously recorded spike time series (n) were discretized into 1ms bins: x_t and n_t denote respectively the stimulus value and spike count (0 or 1) in bin t.

GLMs express how the expected spike count of a unit depends both on the recent stimulus history and on the unit's recent spiking history. The standard functional form of the model we used was:

$$y_t = f\left(\vec{k}^T \overrightarrow{x_t} + \vec{h}^T \overrightarrow{n^*_t} + b\right), \qquad (1)$$

Here n^*_t, the output in bin t, was a Bernoulli (spike or no-spike) random variable. The probability of a spike in bin t, y_t, depended on three terms: (1) the dot product between the stimulus history vector $\overrightarrow{x_t} = (x_{t-Lk+1},\ldots,x_t)$ and a 'stimulus filter' $\vec{k}$ (length L_k = 5ms); (2) the dot product between the spike history vector $\vec{n}^* = (n^*_{t-Lh+1},\ldots,n^*_t)$ and a 'spike history filter' $\vec{h}_t$ (length L_h = 2ms); (3) a constant b, which set the spontaneous firing rate. $f(\cdot)$ was the logistic function $f(z) = (1 + e^{-z})^{-1}$.

To consider whether units might encode multiple sensory variables (e.g., both whisker angle and whisker curvature change), we used a GLM with multiple stimulus history terms, one for each sensory variable:

$$y_t = f\left(\vec{k}_1^T \overrightarrow{x_{t;1}} + \vec{k}_2^T \overrightarrow{x_{t;2}} + \vec{h}_t^T \overrightarrow{n^*} + b\right)$$

Here the indices 1,2 label the sensory variables.

Training and testing of the GLM was done using a cross-validation procedure. For each unit, half of the trials were assigned randomly to a training set and half to a testing set. The training set was used to fit the parameters ($\vec{k}$, $\vec{h}$ and b), while the testing set was used to quantify the similarity between the spike train of the recorded unit and that predicted by the GLM. GLM fitting was achieved by finding the parameter values ($\vec{k}$, $\vec{h}$ and b), which minimized a cost function consisting of the sum of the negative log-likelihood and a regularizing term $-\propto \|\vec{k}\|^2$. For all units, model prediction performance on the test set was robust to variation of α over several orders of magnitude: α was therefore set to a standard value of 0.01. To quantify the performance of the model, the sensory time series of the testing set was used as input to the best-fitting GLM to generate a 'predicted' spike train in response. Both real and predicted spike trains were then smoothed by convolution with a 100ms box-car filter and the similarity between them quantified by the Pearson correlation coefficient (PCC). For each unit, the entire training/testing procedure was repeated for 10 random choices of training/testing set and the final prediction accuracy defined as the median of the 10 resulting PCC values.

To test whether a given 'actual' PCC was statistically significant, we tested the null hypothesis that it could be explained by random firing at the same time-averaged rate as that of the recorded unit. To this end, the recorded spike sequences were randomly shifted by 3000-8000 ms and the training/testing procedure above applied to this surrogate data. This was repeated 10 times and the resulting chance PCCs compared to the actual PCC using a signed-rank test, p=0.0025 (Bonferroni corrected).

Quadratic GLM: To test whether the units might exhibit nonlinear dependence on the stimulus parameters, we adapted the GLM defined above (equation 1) to include quadratic stimulus variables (Rajan et al., 2013). This was important to assess whisker angular

acceleration during free whisking, since a subset of units exhibited U-shaped acceleration tuning functions (Figure 3B). Given a stimulus time series x_t, the quadratic stimulus history vector was $[x_{t-Lk+1},\ldots,x_t,x^2_{t-Lk+1},\ldots,x^2_t]$. Fitting methods were otherwise identical to those detailed above.

Effect of angle-curvature correlations on apparent neuronal stimulus encoding in the passive stimulation protocol: If, in a given recording, sensory variable X correlates with sensory variable Y, a neuron responsive purely to X will tend to appear tuned to Y. To investigate whether such an effect might produce apparent sensitivity to whisker angle in the passive stimulation paradigm, we simulated the response of curvature-tuned neurons to the whisker curvature change time series measured during passive white noise stimulation. To minimise free parameters, constrained GLMs (4 free parameters) were used, sensitive either to instantaneous curvature ($\vec{k} = [\gamma]$) or to its first order derivative ($\vec{k} = \gamma$ [-1 1]), where γ was a signed, gain parameter. Parameters ($\vec{h}$, b, γ) were adjusted to produce two spike trains (one for training, the other for testing) with a realistic white noise induced firing rate (~50 spikes/s; Bale et al., 2013) . We then attempted to predict the simulated, curvature-evoked (training) spike train by fitting GLMs (length 5 stimulus filter, 8 free parameters) using as input either angle or curvature change. Cross-validated model accuracy was computed as the PCC between the predicted spike train and the testing spike train (both smoothed by convolution with a 5 ms box-car).

Effect of single-trial approach on GLM prediction performance: The objective of encoding models, such as GLMs, is to obtain an accurate description of the mapping between a stimulus and the neuronal spike trains it evokes. Since the random component of a neuron's response is inherently unpredictable, the best any model can do is to predict the probability of the spike train. To enable this, encoding models have generally (with few exceptions; Park et

al, 2014) been applied to a 'repeated-trials' paradigm, where a stimulus sequence (e.g., frozen white noise) is repeated on multiple 'trials' (Arabzadeh et al., 2005; Lottem and Azouz, 2011; Bale et al., 2013; Petersen et al., 2008; Pillow et al., 2008). Model accuracy can then be quantified, largely free of contamination from random response variability, by comparing (using PCC or otherwise) the trial-averaged response of the model to the trial-averaged response of the neuron.

In contrast, in the present study of awake, actively whisking mice, the precise stimulus (time series of whisker angle/curvature) was inevitably different on every pole presentation: there were no precisely repeated trials to average over. Our standard model performance metric (PCC) was computed by comparing the response on a single long, concatenated 'trial' to the corresponding GLM predicted response. Such a PCC is downwards biased by random response variability.

To gauge the approximate magnitude of this downward bias, we used a simulation approach. By simulating the response of model neurons, we could deliver identical, repeated trials and, thereby compare model prediction performance by a metric based on trial-averaging with that based on the single-trial approach. To this end, for each recorded unit, we used the best-fitting curvature change GLM to generate 100 trials of spike trains evoked by the curvature time series measured for that unit. Data from the first of these trials was used to fit the parameters of a minimal 'refitted GLM' (stimulus filter length 1, spike history filter length 2; total 4 free parameters), and the single-trial performance quantified, using the approach of the main text (Figure 2-figure supplement 1B, left). Next, we used the refitted GLM to generate 100 repeated trials of spike trains evoked by the curvature time series. Repeated-trials performance was then quantified as the PCC between PSTHs obtained by trial-averaging (Figure 2, -figure supplement 1B right).

470

ACKNOWLEDGEMENTS:

We thank S. Fox, M. Humphries, M.S.E. Loft, R. Lucas and M. Maravall for comments on the manuscript/discussion; K. Svoboda for sharing behavioural methods; G. Caspani, K. Chlebikova, B. Nathanson and R. Twaites for assistance with whisker tracking.

AUTHOR CONTRIBUTIONS:

DC and RSP designed the study. DC and AE performed the experiments. DC, MHE and RSP analyzed the data. MRB, AE, DC and RSP developed the experimental methods. DC, MHE and RSP wrote the manuscript, with input from all authors.

CONFLICT OF INTERESTS:

The authors declare no competing financial interests.

REFERENCES

Abraira VE and Ginty DD. 2013. The sensory neurons of touch. *Neuron* **79**: 618-639. doi:10.1016/j.neuron.2013.07.051

Arabzadeh E, Zorzin E and Diamond ME. 2005. Neuronal encoding of texture in the whisker sensory pathway. *PLoS Biol* **3**:e17. doi: 10.1371/journal.pbio.0030017

Bagdasarian K, Swed M., Knutsen PM, Deutsch D, Derdikman D, Pietr M, Simony E. and Ahissar E. 2013. Pre-neuronal morphological processing of object location by individual whiskers. *Nat Neurosci*, **16**:622-631. doi:10.1038/nn.3378

Bale MR and Petersen RS. 2009. Transformation in the neural code for whisker deflection direction along the lemniscal pathway. *J Neurophysiol* **102:** 2771-2780. doi: 10.1152/jn.00636.2009

Bale MR, Campagner D, Erskine A and Petersen RS. 2015. Microsecond-Scale Timing Precision in Rodent Trigeminal Primary Afferents, *J Neurosci* **35**: 5935-5940. doi: 10.1523/JNEUROSCI.3876-14.2015

Bale MR, Davies K, Freeman OJ, Ince RA and Petersen RS. 2013. Low-dimensional sensory feature representation by trigeminal primary afferents. *J Neurosci* **33**: 12003-12012. doi: 10.1523/JNEUROSCI.0925-13.2013

Birdwell JA, Solomon JH, Thajchayapong M, Taylor, MA, Cheely M, Towal RB, Conradt J and Hartmann MJZ. 2007. Biomechanical models for radial distance determination by the rat vibrissal system. *J Neurophysiol* **98**: 2439–2455. doi: 10.1152/jn.00707.2006

504 Clack NG, O'Connor DH, Huber D, Petreanu L, Hires A, Peron S, Svoboda K, Myers EW.
505 2012. Automated tracking of whiskers in videos of head fixed rodents. *PloS Comput Biol*
506 **8**:e1002591. doi: 10.1371/journal.pcbi.1002591

507 Curtis JC and Kleinfeld D. 2009. Phase-to-rate transformations encode touch in cortical
508 neurons of a scanning sensorimotor system. *Nat Neurosci* **12(4)**: 492-501.

509 Diamond ME, von Heimendahl M, Knutsen PM, Kleinfeld D and Ahissar E. 2008.
510 'Where'and'what'in the whisker sensorimotor system. *Nat Rev Neurosci*, **9(8)**: 601-612.
511 doi:10.1038/nrn2411

512 Fairhall A and Sompolisky H. 2014. Editorial overview: theoretical and computational
513 neuroscience. *Curr Opin Neurobiol* **25**:1:236. doi:10.1016/j.conb.2014.02.010

514 Fox C, Evans M, Pearson M, and Prescott T. 2012. Tactile SLAM with a biomimetic
515 whiskered robot. In IEEE International Conference on in robotics and automation (ICRA),
516 4925-4930.

517 Gibson JJ. 1962. Observations on active touch. *Psychological Rev* **69**: 477-491.

518 Gibson JM. and Welker WI. 1983. Quantitative studies of stimulus coding in first-order
519 vibrissa afferents of rats. 1. Receptive field properties and threshold distributions. *Somatosens*
520 *Mot Res* **1**:51-67. doi: 10.3109/07367228309144540

521 Hubel DH. 1959. Single unit activity in striate cortex of unrestrained cats. *J physiol*. **147.2**:
522 226-238. doi: 10.1113/jphysiol.1959.sp006238

523 Huber D, Gutnisky D, Peron S, O'Connor DH, Wiegert J. S., Tian L., Oertner T. G., Looger
524 L. L., and Svoboda K. 2012. Multiple dynamic representations in the motor cortex during
525 sensorimotor learning. *Nature* **484:** 473-478. doi: 10.1038/nature11039

526 Jones LM, Depireux DA, Simons DJ and Keller A. 2004. Robust temporal coding in the
527 trigeminal system. *Science* **304**: 1986-1989. doi: 10.1126/science.1097779

528 Khatri V, Bermejo R, Brumberg JC, Keller A. and Zeigler HP. 2009. Whisking in air:
529 encoding of kinematics by trigeminal ganglion neurons in awake rats. *J Neurophysiol* **101**:
530 1836-1846. doi: 10.1152/jn.90655.2008.Kleinfeld D and Deschênes M. 2011. Neuronal basis
531 for object location in the vibrissa scanning sensorimotor system. *Neuron* **72**:455-468. doi:
532 10.1016/j.neuron.2011.10.009.

533 Knutsen PM, Biess A and Ahissar W. 2008. Vibrissal kinematics in 3D: tight coupling of
534 azimuth, elevation, and torsion across different whisking modes. *Neuron* **59**: 35-42.

535 Leiser SC and Moxon, KA. 2007. Responses of trigeminal ganglion neurons during natural
536 whisking behaviors in the awake rat. *Neuron* **53**: 117-133. doi:10.1016/j.neuron.2006.10.036.

537 Lettvin JY, Maturana HR, McCulloch WS and Pitts WH. 1959. What the frog's eye tells the
538 frog's brain. *Proc. IRE* **47**: 1940-1951.

539 Lewen GD, Bialek W, Steveninck RRDRV. Neural coding of naturalistic motion stimuli.
540 *Network* **12(3)**: 317:329.

541 Lichtenstein SH, Carvell GE, and Simons DJ. 1990. Responses of rat trigeminal ganglion
542 neurons to movements of vibrissae in different directions. *Somatosens Mot Res* **7**: 47-65. doi:
543 1 0.1152/jn.90511.2008.

544 Lottem E and Azouz R. 2011. A unifying framework underlying mechanotransduction in the
545 somatosensory system. *J Neurosci* **31**: 8520-8532. doi: 10.1523/JNEUROSCI.6695-10.2011.

546 Mante V, Bonin V and Carandini M. Functional mechanisms shaping lateral geniculate
547 responses to artificial and natural stimuli. *Neuron* **58**: 625-638. doi:
548 10.1016/j.neuron.2008.03.011

549 Nelder JA and Wedderburn RWM. 1972. Generalized linear models. *J R Statist Soc Ser A*,
550 **135**: 370–384.

551 O'Connor DH, Clack NG, Huber D, Komiyama T, Myers EW and Svoboda K. 2010a.
552 Vibrissa-based object localization in head-fixed mice. *J Neurosci* **30**: 1947-1967. doi:
553 10.1523/JNEUROSCI.3762-09.2010.

554 O'Connor DH, Peron SP, Huber D and Svoboda K. 2010b. Neural activity in barrel cortex
555 underlying vibrissa-based object localization in mice. *Neuron*, **67**: 1048-1061. doi:
556 http://dx.doi.org/10.1016/j.neuron.2010.08.026.

557 Pammer L, O'Connor DH, Hires SA, Clack NG, Huber D, Myers EW and Svoboda K. 2013.
558 The mechanical variables underlying object localization along the axis of the whisker. *J*
559 *Neurosci*, **33**: 6726-6741. doi: 10.1523/JNEUROSCI.4316-12.2013.

560 Paninski L, Pillow J and Lewi J. 2007. Statistical models for neural encoding, decoding, and
561 optimal stimulus design. *Prog Brain Res*, **165**: 493-507.doi:10.1016/S0079-6123(06)65031-0

562 Park IM, Meister ML, Huk AC and Pillow JW. 2014. Encoding and decoding in parietal
563 cortex during sensorimotor decision-making. *Nat Neurosci*. **17**: 1395-1403. doi:
564 doi:10.1038/nn.3800

565 Pearson MJ, Fox C, Sullivan JC, Prescott TJ, Pipe T and Mitchinson B. 2013. Simultaneous
566 localization and mapping on a multi-degree of freedom biomimetic whiskered robot. In IEEE

International Conference on robotics and automation (ICRA), 586-592. doi: 10.1109/ICRA.2013.6630633

Perkon I, Košir A, Itskov PM, Tasič J and Diamond ME. 2011. Unsupervised quantification of whisking and head movement in freely moving rodents. *J Neurophysiol* **105:** 1950-1962. doi: 10.1152/jn.00764.2010.

Peron SP, Freeman J, Iyer V, Guo C and Svoboda K. 2015. A Cellular Resolution Map of Barrel Cortex Activity during Tactile Behavior. *Neuron* **86**: 783-799. doi: 10.1016/j.neuron.2015.03.027

Petersen RS, Brambilla M, Bale MR, Alenda A, Panzeri S, Montemurro MA and Maravall M. 2008. Diverse and temporally precise kinetic feature selectivity in the VPm thalamic nucleus. *Neuron* **60**: 890–903. doi: 10.1016/j.neuron.2008.09.041.

Petreanu L, Gutnisky D, Huber D, Xu N, O'Connor D, Tian L, Looger L and Svoboda K. 2012. Activity in motor-sensory projections reveals distributed coding in somatosensation. *Nature* **489**: 299-303. doi: 10.1038/nature11321.

Phillips JR and Johnson KO. 1981. Tactile spatial resolution. III. A continuum mechanics model of skin predicting mechanoreceptor responses to bars, edges, and gratings. *J Neurophysiol*, **46**: 1204-1225.

Pillow JW, Shlens J, Paninski L, Sher A, Litke AM, Chichilnisky EJ and Simoncelli EP. 2008. Spatio-temporal correlations and visual signalling in a complete neuronal population. *Nature* **454**: 995-999. doi: 10.1038/nature07140.

587 Poole K, Moroni M, and Lewin GR. 2015. Sensory mechanotransduction at membrane-
588 matrix interfaces. *Pflügers Archiv-European J Physiol*, **467**: 121-132. doi: 10.1007/s00424-
589 014-1563-6

590 Quist BW and Hartmann MJ. 2012. Mechanical signals at the base of a rat vibrissa: the effect
591 of intrinsic vibrissa curvature and implications for tactile exploration. *J Neurophysiol*, **107**:
592 2298–2312. doi: 10.1152/jn.00372.2011.

593 Quist BW, Seghete V, Huet LA, Murphey TD, & Hartmann MJ. 2014. Modeling forces and
594 moments at the base of a rat vibrissa during noncontact whisking and whisking against an
595 object. *J Neurosci*, **34(30)**: 9828-9844.

596 Rajan K, Marre O and Tkačik G. 2013. Learning quadratic receptive fields from neural
597 responses to natural stimuli. *Neural Comp*, **25**: 1661-1692. doi: 10.1162/NECO_a_00463.

598 Reinagel P. 2001. How do visual neurons respond in the real world? *Curr Opin Neurobiol*,
599 **11(4)**: 437-442. doi:10.1016/S0959-4388(00)00231-2

600 Rice FL, Mance A and Munger BL. 1986. A comparative light microscopic analysis of the
601 sensory innervation of the mystacial pad. I. Innervation of vibrissal follicle-sinus complexes.
602 *J Compa Neurol*, **252(2)**: 154-174.

603 Simoncelli EP and Olshausen BA. 2001, Natural image statistics and neural representation,
604 *Ann Rev Neurosci*, **24**: 1193-1216. doi: 10.1146/annurev.neuro.24.1.1193.

605 Sofroniew NJ, Cohen JD, Lee AK, and Svoboda K. 2014. Natural whisker-guided behavior
606 by head-fixed mice in tactile virtual reality. *J Neurosci*, **34**: 9537-9550. doi:
607 10.1523/JNEUROSCI.0712-14.2014.

608 Solomon JH and Hartmann MJZ. 2006. Biomechanics: robotic whiskers used to sense
609 features. *Nature* **443**: 525-525. doi: 10.1038/443525a.

610 Szwed M, Bagdasarian K and Ahissar E. 2003. Encoding of vibrissal active touch. *Neuron*,
611 **40**: 621–630. doi:10.1016/S0896-6273(03)00671-8.

612 Szwed M, Bagdasarian K, Bluenfeld B, Barak O, Derdikman D and Ahissar E. 2006.
613 Responses of trigeminal ganglion neurons to the radial distance of contact during active
614 vibrissal touch. *J Neurophysiol*, **95**: 791-802. doi: 10.1152/jn.00571.2005.

615 Truccolo W, Eden UT, Fellows MR, Donoghue JP and Brown EN. 2005. A point process
616 framework for relating neural spiking activity to spiking history, neural ensemble, and
617 extrinsic covariate effects. *J Neurophysiol* **93**: 1074–1089. doi: 10.1152/jn.00697.2004.

618 Whiteley,SJ, Knutsen PM, Matthews DW and Kleinfeld D. 2015. Deflection of a vibrissa
619 leads to a gradient of strain across mechanoreceptors in a mystacial follicle. *J Neurophysiol*
620 ***66***: 67. doi: 10.1152/jn.00179.2015.

621 Woo S-H et al., 2014. Piezo2 is required for Merkel-cell mechanotransduction. *Nature* **509**:
622 622-626. doi:10.1038/nature13251.

623 Yarbus AL. 1967. Eye movements and vision. New York: Plenum Press.

624 Zucker E and Welker WI. 1969. Coding of somatic sensory input by vibrissae neurons in the
625 rat's trigeminal ganglion. *Brain Res* **12**: 138-156. doi:10.1016/0006-8993(69)90061-4

626

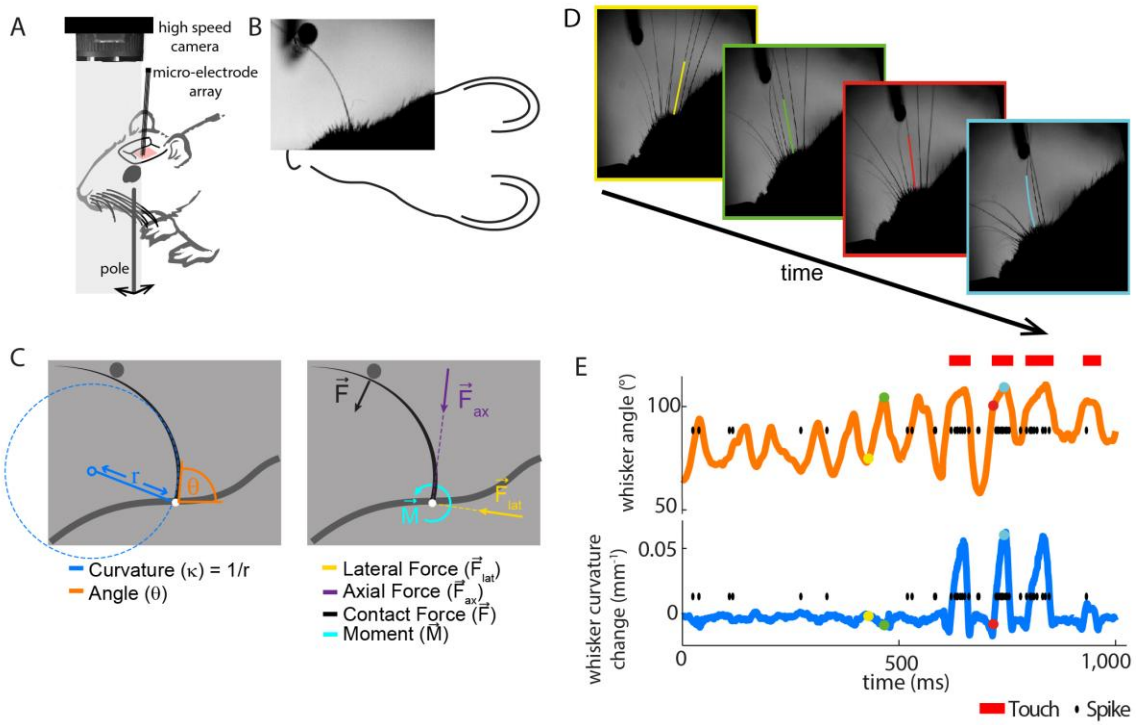

627

628 **Figure 1. Electrophysiological recording from single primary whisker units in awake,**

629 **head-fixed mice and simultaneous measurement of whisker kinematics/mechanics.**

630 **A.** Schematic of the preparation, showing a tungsten microelectrode array implanted into the

631 trigeminal ganglion of a head-fixed mouse, whilst a metal pole is presented in one of a range

632 of locations (arrows). Before the start of each trial, the pole was moved to a randomly

633 selected, rostro-caudal location. During this time, the whiskers were out of range of the pole.

634 At the start of the trial, the pole was rapidly raised into the whisker field, leading to whisker-

635 pole touch. Whisker movement and whisker-pole interactions were filmed with a high-speed

636 camera.

637 **B and C.** Kinematic (whisker angle θ) and mechanical (whisker curvature κ, moment $\vec{M}$,

638 axial force $\vec{F}_{ax}$ and lateral force $\vec{F}_{lat}$) variables measured for the principal whisker in each

639 video frame.

D. Individual video frames during free whisking (yellow and green) and whisker-pole touch (red and cyan) with tracker solutions for the target whisker (the principal whisker for the recorded unit, panel **E**) superimposed (coloured curve segments).

E. Time series of whisker angle and curvature change, together with simultaneously recorded spikes (black dots) and periods of whisker-pole contact (red bars). Coloured dots indicate times of correspondingly coloured frames in **D**.

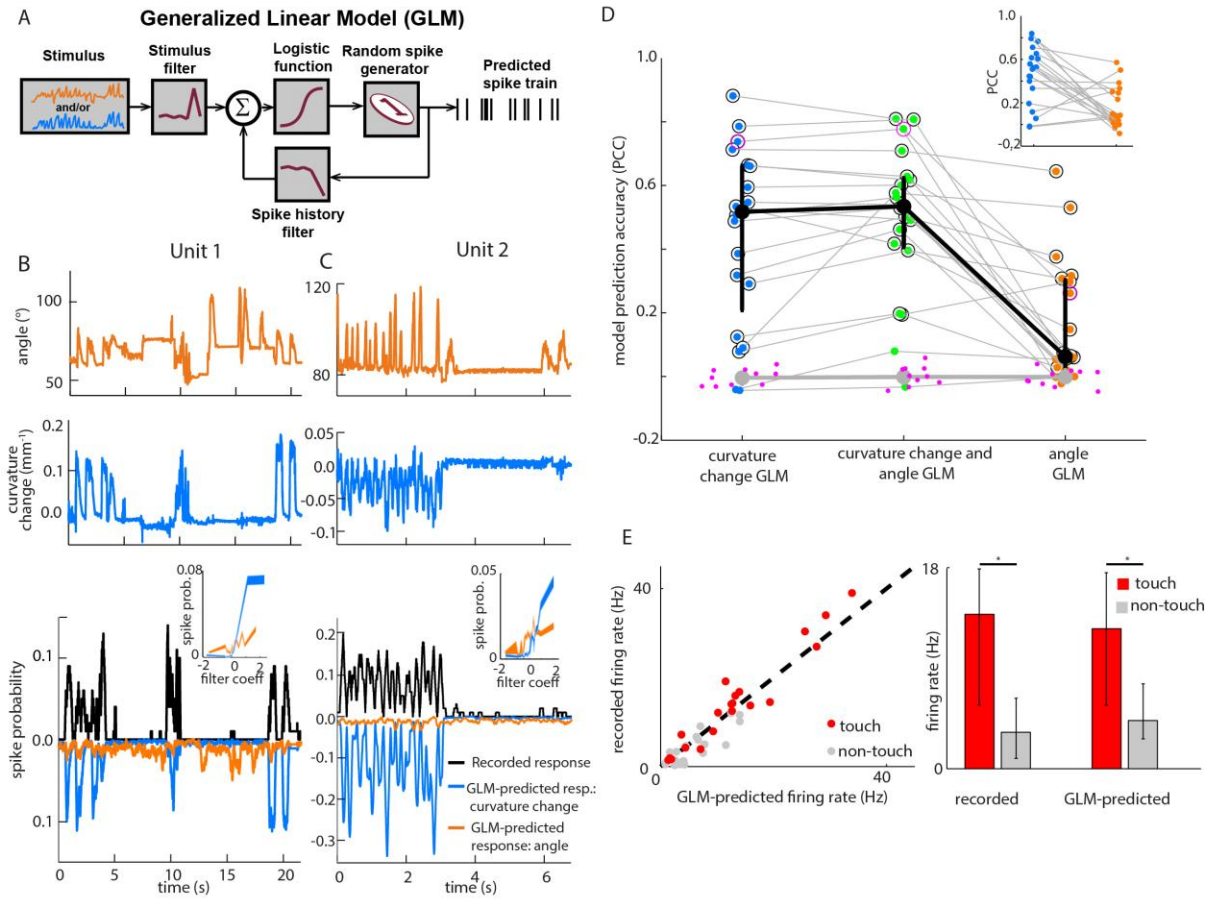

Figure 2. Primary whisker neurons encode whisker curvature, not whisker angle, during active sensation.

A. Schematic of the Generalized Linear Model (GLM).

B. For an example unit, whisker angle (top panel), whisker curvature change (middle panel) and simultaneously recorded spike train (bottom panel, black), together with predicted spike trains for the best-fitting angle GLM (bottom panel, orange) and curvature change GLM (bottom panel, blue). Spike trains discretized using 1 ms bins and smoothed with a 100 ms boxcar filter. Prediction performance (Pearson correlation coefficient, PCC) for this unit was 0.59. Inset shows tuning curves for both GLMs, computed by convolving the relevant sensory time series (angle or curvature change) with the corresponding GLM stimulus filter to produce a time series of filter coefficients, and estimating the spiking probability as a function of filter coefficient (25 bins).

667 **C**. Analogous to panel **B** for a second example unit. Prediction performance PCC for this unit
668 was 0.74.

669 **D.** Prediction performance between predicted and recorded spike trains) compared for GLMs
670 fitted with three different types of input: curvature change alone; angle alone; both curvature
671 change and angle. Each blue/orange/green dot is the corresponding PCC for one unit: large
672 black dots indicate median; error bars denote inter-quartile range (IQR). To test statistical
673 significance of each unit's PCC, the GLM fitting procedure was repeated 10 times on spike
674 trains subjected each time to a random time shift: magenta dots show these chance PCCs for
675 the unit indicated by the magenta circle; the mean chance PCC was computed for each unit,
676 and the large gray dot shows the median across units. Black circles indicate units whose PCC
677 was significantly different to chance (signed-rank test, Bonferroni corrected, $p<0.0025$). To
678 facilitate direct comparison between results for curvature change GLM and angle GLM, these
679 are re-plotted in the inset.

680 **E. Left.** Firing rate during touch episodes compared to that during non-touch episodes for
681 each unit, compared to corresponding predicted firing rates from each unit's curvature change
682 GLM. **Right.** Medians across units: error bars denote IQR; * denotes differences significant
683 at $p<0.05$ (signed-rank test).

684

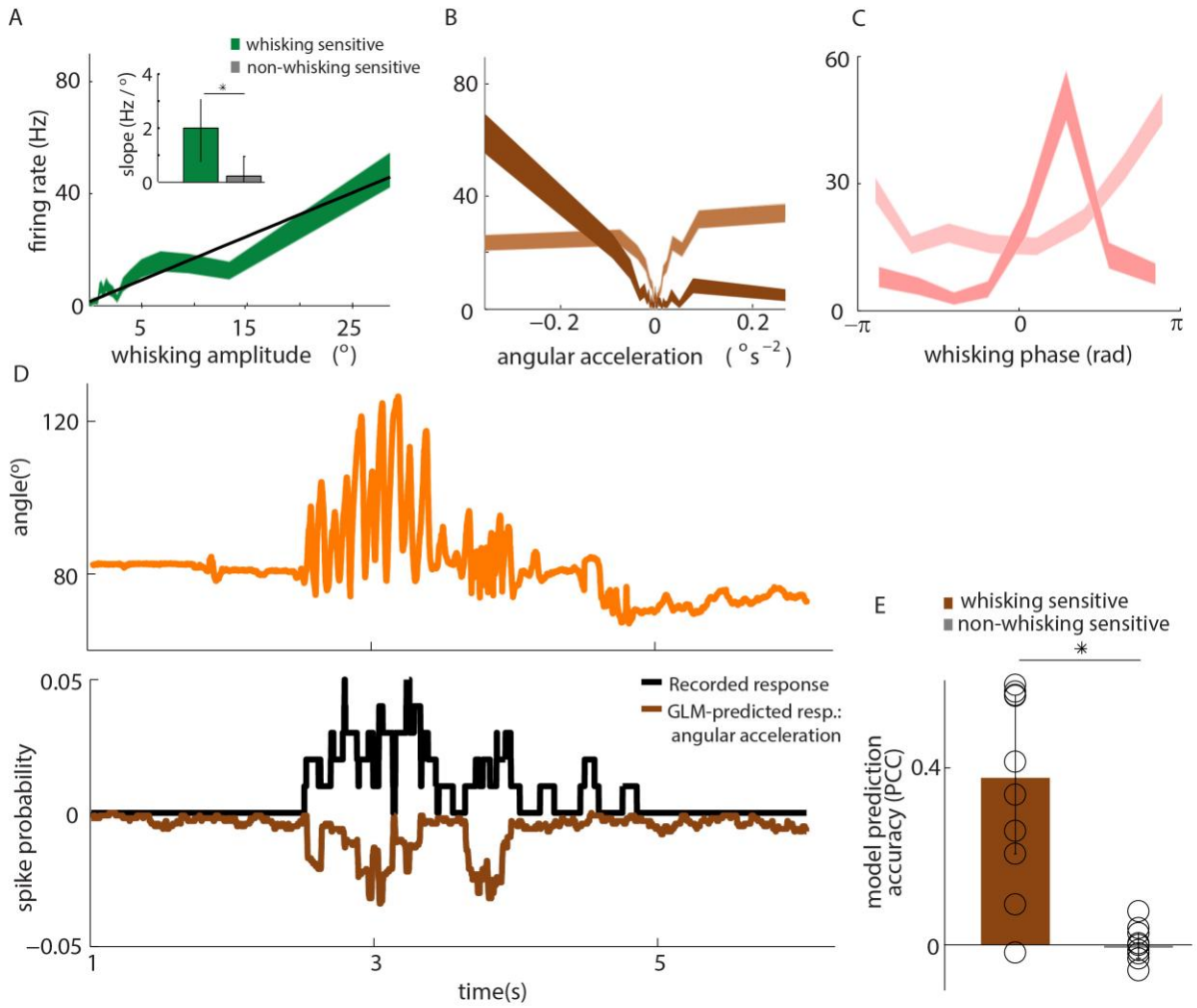

Figure 3. Primary whisker neurons encode whisker angular acceleration during free whisking

A. Mean response of an example whisking-sensitive unit to whisking amplitude, computed during non-contact episodes (dark green, shaded area shows SEM) with regression line (black). Inset shows regression line slopes (median and IQR) for whisking sensitive (green) and non-whisking sensitive (grey) units. * indicates statistical significance rank-sum test (p=0.05).

B. Mean response of two example units as a function of angular acceleration. The dark brown unit is the same as that shown in A.

C. Mean response of two example units as a function of whisking phase. The dark pink unit is the same as that reported in A; the light pink unit is the same as that shown as light brown in B.

D. An excerpt of free whisking (**orange)** along with activity of an example, whisking-sensitive unit (black) and activity predicted by a GLM driven by angular acceleration (brown). The unit is the same as that shown in **A**.

E.GLM prediction accuracy (PCC) for all whisking sensitive (brown) and whisking insensitive units (grey). Bars and vertical lines denote median and IQR respectively.

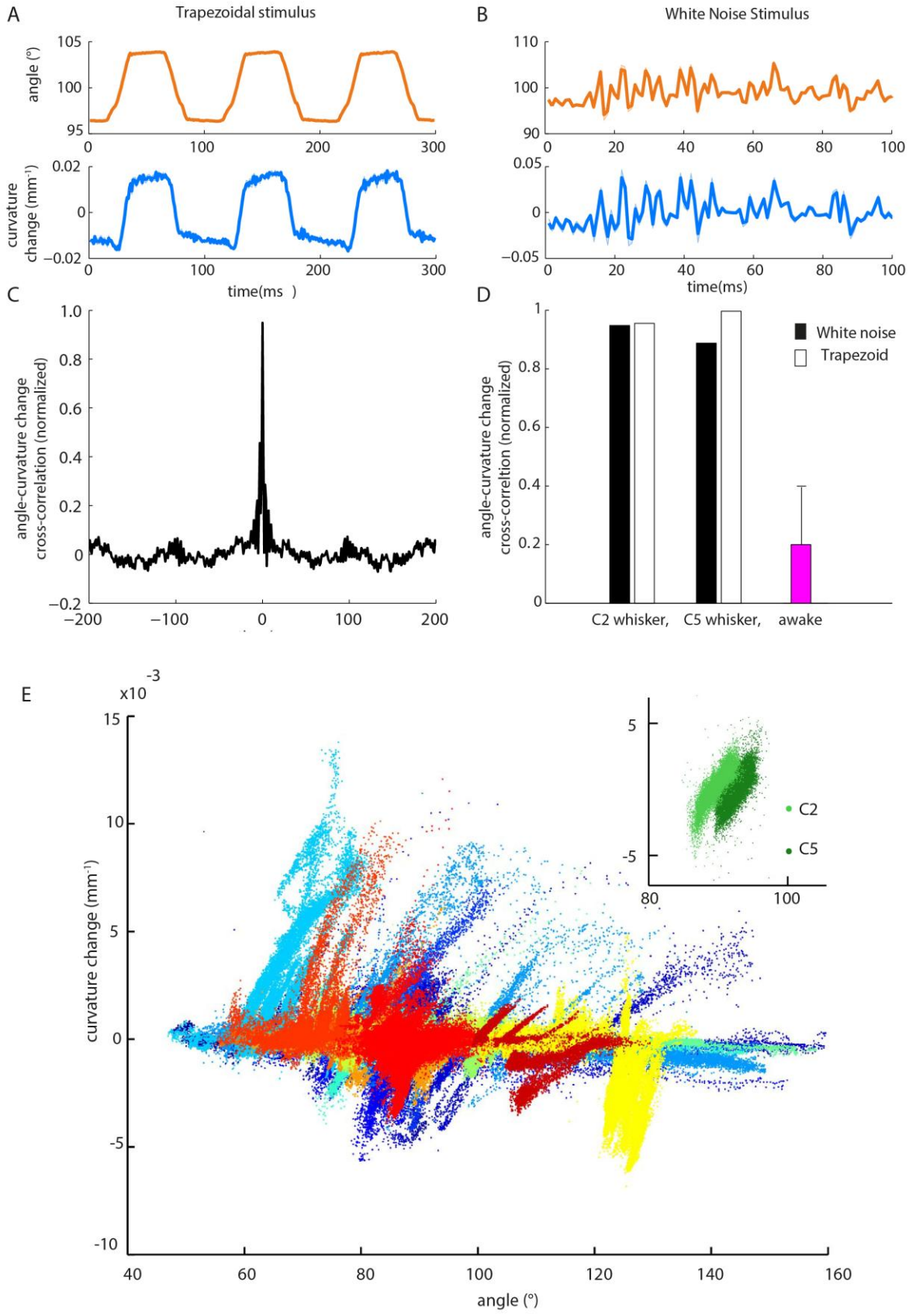

716

Figure 4. Whisker angle and whisker curvature change are highly correlated during passive whisker deflection, but decoupled during active touch.

A. Whisker angle (**top**) and whisker curvature change (**bottom**) time series, due to passive, trapezoidal stimulation of C2 whisker in an anaesthetised mouse, estimated as mean over 10 repetitions. Note that errorbars (showing SEM) are present but very small.

B. Corresponding data for low-pass filtered white noise (hereafter abbreviated to 'white noise') stimulation of the same whisker.

C. Cross-correlation between curvature change and angle during white noise stimulation, for C2 whisker.

D. Cross-correlation between angle and curvature change at zero lag, for both passive stimulation under anaesthesia and awake, active sensing (median of absolute cross-correlation for each unit; error bar denotes IQR).

E. Joint distribution of whisker angle and whisker curvature change in awake, behaving mice (1 ms sampling). Different colours denote data corresponding to different recorded units. **Inset**: Analogous plot for passive, white noise whisker deflection in an anaesthetised mouse. Different colours indicate data from different whiskers.

738 **SUPPLEMENT**

739

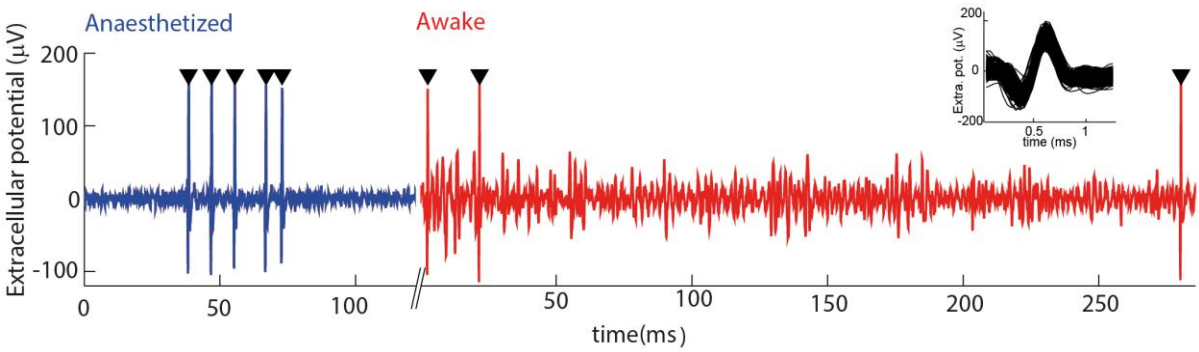

740

741 **Figure 1-figure supplement 1. Electrophysiological recording from trigeminal primary**

742 **neurons of awake, head-fixed mice.**

743 Extracellular potential recorded from the same single unit during both anaesthetized and

744 awake epochs. Spikes belonging to the cluster of the target unit are shown by black triangles.

745 Inset shows overlay of all waveforms belonging to this cluster.

746

747

748

749

750

751

752

753

754 **Figure 1- figure supplement 2: Video of an awake mouse, exploring a pole with its**

755 **whiskers with simultaneous electrophysiological recording of a primary whisker neuron**

756 High-speed video of a head-fixed mouse (1000 frames/s) with sound of spikes fired by a

757 primary whisker unit. The pole is initially out of range of the whiskers. Whisker tracker

758 solution for the principal whisker of the recorded unit is overlaid in red.

759

760

761

762

763

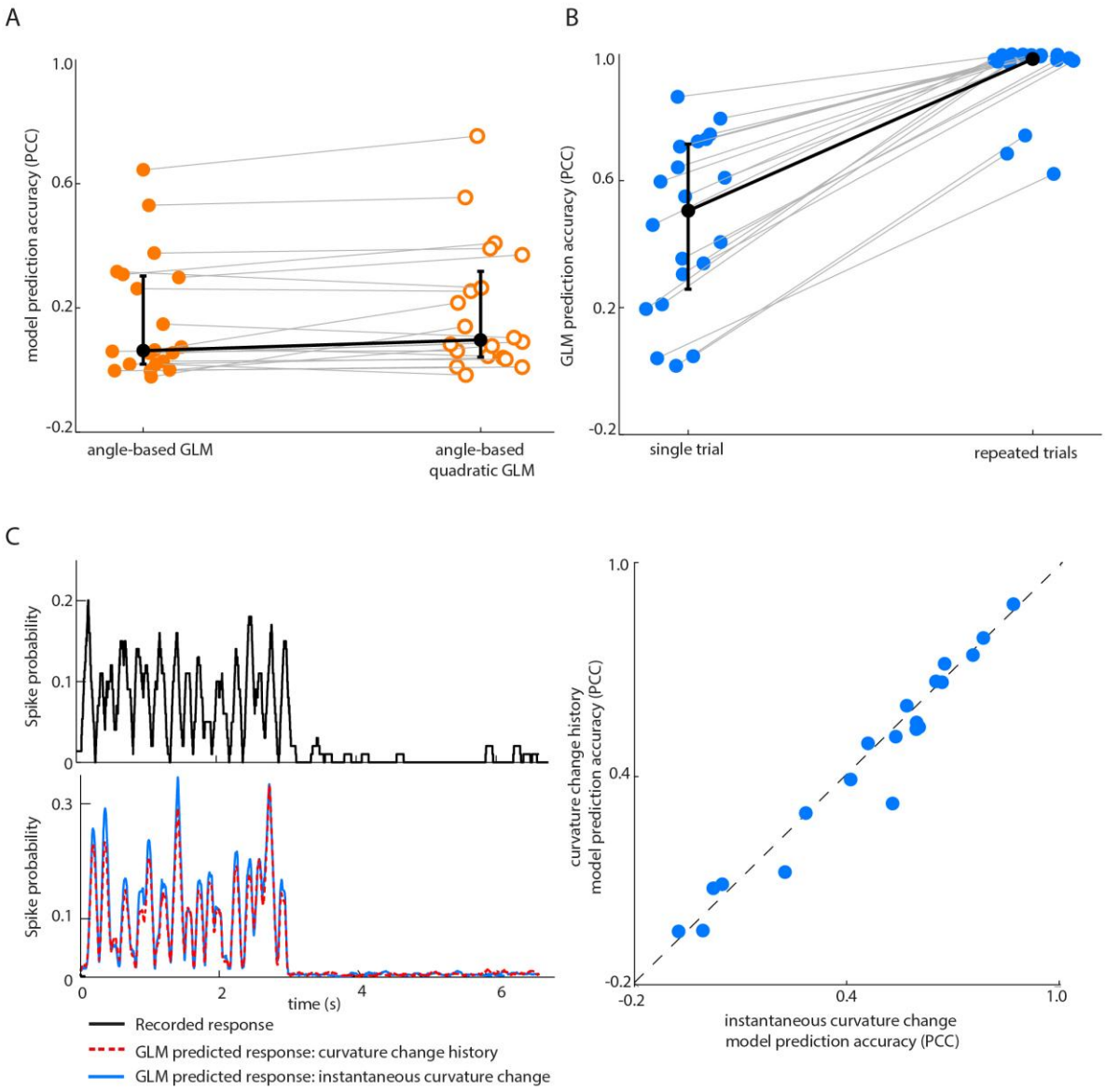

764

765

766 **Figure 2- figure supplement 1. Effect on GLM performance of quadratic input terms,**

767 **simulated repeated trials and minimal stimulus filters**

768 **A.** Angle GLM prediction performance is robust to addition of quadratic stimulus-

769 dependence. Prediction accuracy (PCC) for standard angle GLM (same data as Figure 2C of

770 main text) in comparison to quadratic GLM (see Methods). Black dots denote medians, error

771 bars IQR.

B. Single-trial GLM prediction accuracy is limited by neuronal response variability. Prediction accuracy (PCC) for simulated neurons. Each simulated neuron is the best-fitting GLM, based on instantaneous curvature change, for its corresponding recorded unit (see Methods). Prediction accuracy is quantified both using the single-trial approach of the main text and using a repeated-trial method only possible by virtue of using a simulation. Black dots denote medians, error bars IQR.

C. Prediction accuracy of curvature-based GLMs is accounted for by tuning to instantaneous curvature change. A GLM performs a temporal filtering operation on its sensory stimulus input and the sensory feature(s) which it encodes is determined by this 'stimulus filter'. The stimulus filters can, in principle, be complex, but we found that the ability of a GLM to predict spikes (**lower left**) from curvature change was fully explained by the simple case where the action of the stimulus filter is simply to multiply the sensory input by a gain factor (median 0.55, IQR 0.26-0.66; p=0.35 signed-rank test). Recorded spike train (**upper left**) and curvature-predicted spike trains (**lower left**) both for a 'curvature history' GLM with a length 5 stimulus filter identical to Figure 2D of main text and for an 'instantaneous curvature' GLM with a length 1 stimulus filter. Data for unit 2 of main text Figure 2C. Prediction accuracy of the curvature history GLM compared to that of the instantaneous curvature GLM for every recorded unit (**right**).

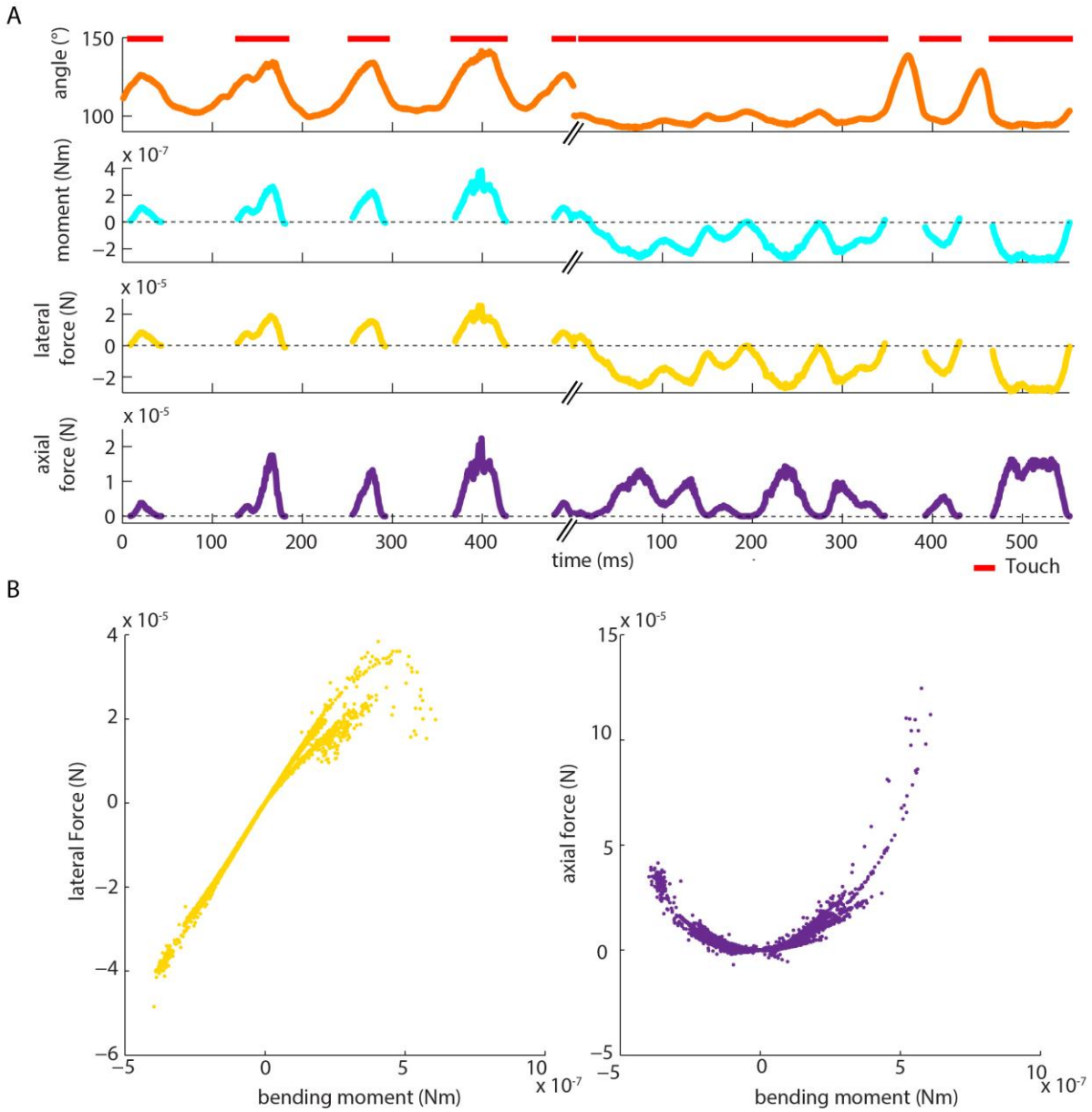

Figure 2- figure supplement 2. Moment is near-perfectly correlated with axial/lateral contact force components during pole exploration.

A. Two example time series for simultaneously measured whisker angle, bending moment, lateral force and axial force (see Methods). Red bars indicate episodes of whisker-pole contact.

B. Joint distribution of bending moment and lateral force (**left**), compared to that of bending moment and axial force (**right**), for the same recording shown in **A**. Moment was highly

798 linearly correlated with lateral force (median absolute correlation coefficient across units
799 0.995, IQR 0.987-0.999, median R^2 of linear fit 0.99, IQR 0.97-1.0), and highly quadratically
800 correlated with axial force (median R^2 of quadratic fit 0.94, IQR 0.85-0.98). This indicates
801 that, during our conditions of pole exploration, axial force and lateral force are both
802 redundant with moment.

803

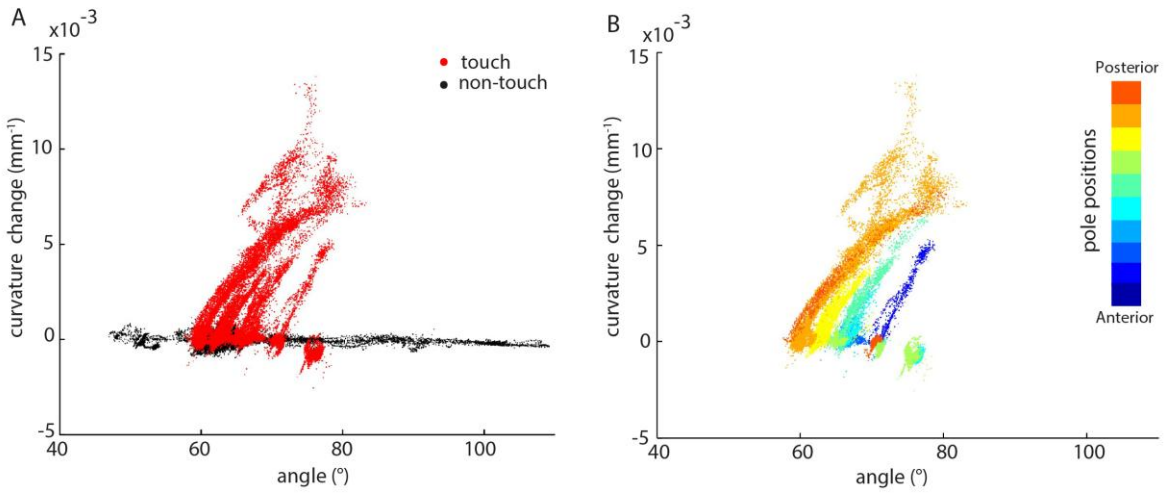

804

805 **Figure 4-figure supplement 1. Natural statistics of active touch are rich: relationship**

806 **between whisker angle and whisker curvature change.**

807 **A.** Joint distribution of angle and curvature change for an example recording from an awake

808 behaving mouse, with samples registered during touch and non-touch distinguished by colour

809 (1 ms sampling).

810 **B.** Touch data of **A** classified according to pole position (dot colour).

811

812

813

814

815

816

817

818

819

820

821

822

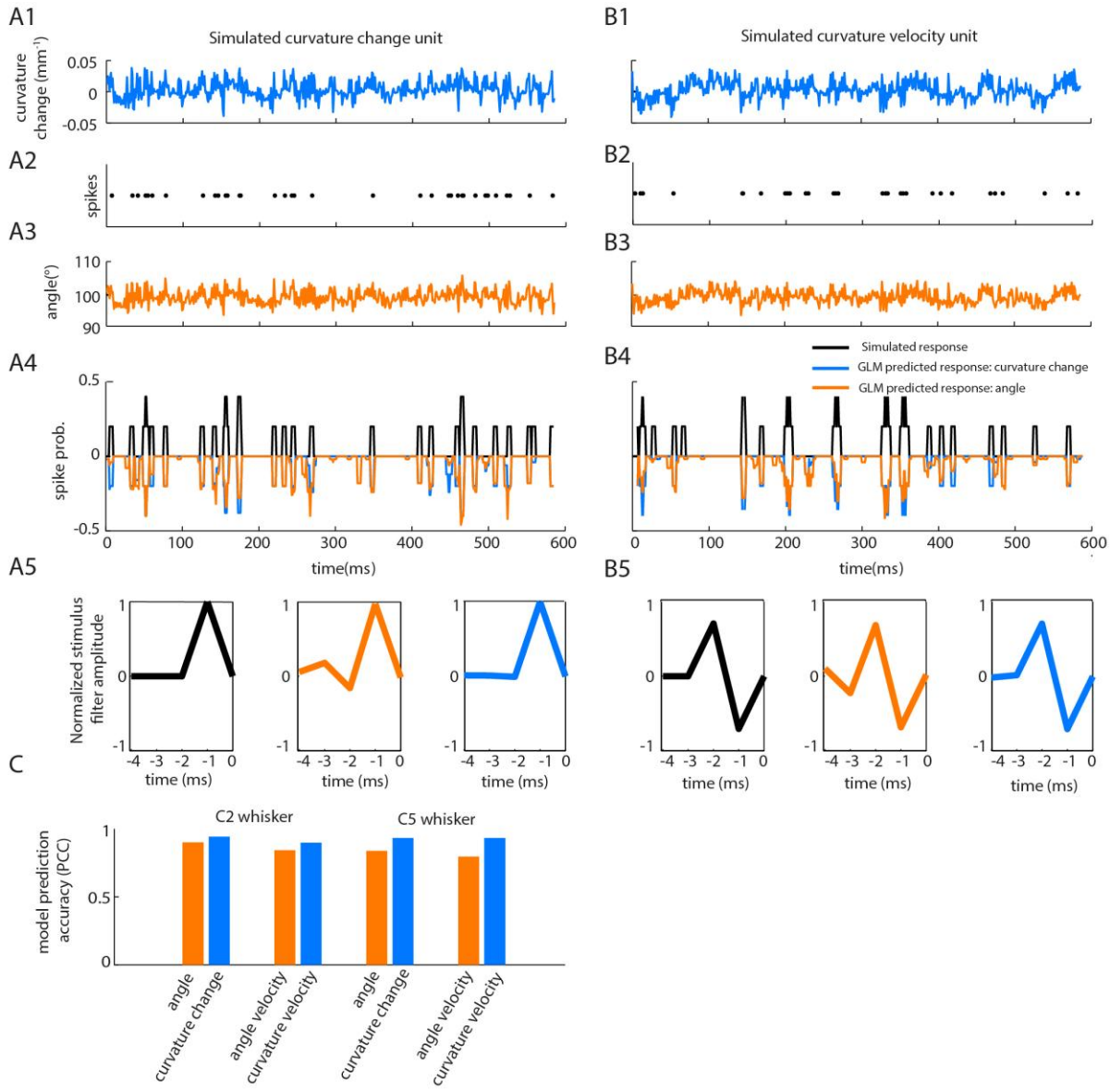

Figure 4-figure supplement 2: Correlations between angle and curvature change during passive whisker stimulation can make curvature-tuned units appear angle-tuned.

The data of Figure 4 show a strong correlation between whisker angle and whisker curvature during passive stimulation of the whisker. To test whether this correlation might make curvature-tuned units appear angle-tuned, we used a simulation approach. This allowed us to generate responses from idealised neurons whose true tuning was known, by construction, to be only to curvature. We simulated responses of such neurons to the curvature change time series obtained from passive white noise stimulation (**A1-2**). We then trained a GLM to

predict these curvature-evoked spikes using only whisker angle as input (**A3-A4**). Despite being fed the 'wrong' input, this GLM was able to predict the spikes accurately (for C2 whisker, angle PCC was 0.90, curvature change PCC 0.94; results similar for C5; **C**). This result was robust to different choices of feature tuning (**B-C**).

A1. Whisker curvature change caused by the white noise stimulus applied to C2 whisker of an anaesthetized mouse (same data as main text Figure 3, repeated for clarity).

A2. Spike train evoked by a simulated curvature-tuned neuron in response to the stimulus in A1 (a GLM with the position filter shown in left panel of A5).

A3. Whisker angle time series corresponding to panel A1.

A4. Target response (black) compared to predicted response from best-fitting GLMs using either angle (orange) or curvature change (blue) as input.

A5. **Left**. Stimulus filter used to generate the spike train of panel A2. **Middle-Right**. Best-fitting stimulus filters (normalised to unit length) for GLMs trained on the spikes of panel A2 and the angle time series of panel A3 or the curvature change time series of panel A1 respectively.

B1-5. Results analogous to A1-5 for a simulated neuron tuned to curvature velocity.

C. Quantification of the GLM predictions shown in panels A4-B4.